NUMERICAL SIMULATION OF AN OSCILLATING FREESTREAM FLOW AROUND A NACA 0012 AIRFOIL USING THE VORTEX METHOD

Angelo Alberto Mustto, mustto@cepel.br
Departamento de Tecnologias Especiais (DTE) – CEPEL/ELETROBRAS, Av. Horácio Macedo 354, Cidade Universitária, 21941-911 Rio de Janeiro, RJ – BRAZIL

Daniel Fonseca de Carvalho e Silva, danielfc@petrobras.com.br
CENPES/PDP/MC – PETROBRAS, Av. Horácio Macedo 950 - Prédio 32 - 2o andar, Cidade Universitária - Ilha do Fundão, 21941-915 Rio de Janeiro, RJ – BRAZIL

Gustavo Cesar Rachid Bodstein, gustavo@mecanica.coppe.ufrj.br
Department of Mechanical Engineering – Politécnica/COPPE, Federal University of Rio de Janeiro; Centro de Tecnologia, Bloco G, sala 204 – Ilha do Fundão, 21945-970 Rio de Janeiro, RJ – BRAZIL

Abstract. *The Vortex Method has become a powerful numerical mesh-free technique to simulate unsteady incompressible flows characterized by separation and vortex shedding, such as external flows around bluff and streamlined bodies. In this paper, a fully lagrangian vortex method is used to simulate the incompressible two-dimensional oscillating flow around a NACA 0012 airfoil. Piecewise-continuous linear-vortex flat panels are used to represent the body surface and a cloud of Lamb vortices is used to model the vorticity field in the boundary layer and wake. The induced velocities are calculated using the Biot-Savart law and the vortices are convected using the Adams-Bashforth second-order time-marching scheme. The vorticity transport by diffusion is simulated using the Random-Walk method. Numerical simulations are carried out for several values of Keulegan-Carpenter number, KC, and nondimensional excitation frequency,* f_e*. Our results, obtained for a Reynolds number equal to* 1.7×10^5*, show that the amplitude of oscillation increases as the value of KC and* f_e *increase. This behavior is linear for the lower values and non-linear for the higher values of KC and* f_e*. We also observe that the vortex shedding frequency is equal to the excitation frequency in all cases studied. For the higher values of KC used in the simulations, the boundary layer undergoes a large temporal variation, going from attached to massively separated conditions when the local angle of attack reaches high values. This behavior is similar to dynamic stall.*

Keywords*: vortex method, oscillating flow, dynamic stall, unsteady aerodynamics, airfoil.*

1. INTRODUCTION

Oscillatory flows around bluff and streamlined bodies have many engineering applications. If the body is rigid and kept fixed and the freestream flow is uniform, or present periodic components due to upstream turbulence or some periodic perturbation, the flow becomes oscillatory due to the periodic vortex shedding mechanism that results from boundary layer separation. Such flows occur very often in cross-flow heat exchangers and stalled airfoils of wings and turbomachine blades. On the other hand, if the freestream flow is uniform but the body has some prescribed periodic motion, or it is flexible enough to respond to the vortex shedding mechanism with an oscillatory motion, the flow as a whole again experiences an oscillatory interaction between the fluid and the body, causing the development of periodic forces. This latter situation is typical of risers of offshore platforms, power lines exposed to the wind and flapping airfoils of helicopter or wind turbine blades. All these problems involve a variety of forces that arise from fluid-structure interactions, such as the inertial and elastic forces acting on the solid, and the inertial, viscous, pressure and gravitational forces acting on the fluid. In the case of flexible streamlined bodies, the flow is even more complex because the fluid-structure interaction presents characteristics that combine lift generation mechanisms with oscillatory separation, periodic force development and the possible occurrence of lock-in. The phenomenon of "lock-in" is classically defined as the regime where the frequency of oscillation, as well as the vortex formation frequency, are close to the natural frequency of the structure throughout the regime of large-amplitude vibration (Williamson and Govardhan, 2004). In addition, the oscillatory motion of a streamlined body may bring about another unsteady phenomenon that is associated with stall delay, called "dynamic stall". This phenomenon occurs when the airfoil undergoes a pitching motion through the static stall angle and the normal force increases beyond its maximum value for unstalled conditions, dropping off at an angle of attack considerably higher than the static stall angle (Akbari and Price, 2003). Dynamic stall is related to the leading-edge vortex that is formed when the airfoil increases its angle of attack towards a high value, creating suction and producing unsteady aerodynamics forces. The dynamic stall phenomenon was first observed in helicopters, although it also occurs on axial-flow compressors and modern fighters in fast-pitching maneuvers. Blade sections of horizontal-axis wind turbine rotors are also routinely subject to these oscillatory loads.

We here consider a situation where a typical two-dimensional streamlined body, such as an airfoil of a horizontal-axis wind turbine, is immersed in an incoming freestream flow that has periodic components. Particularly, the rotor blades of horizontal-axis wind turbines are designed to operate in ideal conditions; however, in most cases, the turbine

is subject to the action of an incoming wind with high turbulent intensity, which means that the flow presents a remarkable oscillatory component. This oscillatory characteristic is typical of the atmospheric boundary layer flow that generates the wind. In this case, the blades remain subject to a lateral motion in the crossflow plane that contains the airfoil section. Because real three-dimensional wind turbine blades are very long and flexible, they deform and acquire lateral motions due to the action of this oscillatory wind. We simplify our analysis by assuming that the airfoil is rigid and fixed and that the periodic excitation comes from an oscillatory incoming freestream flow, as shown in Fig. 1. We set the geometrical angle of attack angle to a specified value but the flow that develops causes a periodic change of the effective angle of attack, producing a cyclic variation of the effective pitch angle. The periodic behavior of the incident flow induces additional mechanical loads on the blades and a considerable variation of the output power of the turbine.

In this paper, we simulate numerically the flow described above using the Vortex Method (VM). The VM has been extensively used over the last decades for the simulation of incompressible viscous flows and it has become an interesting alternative to the more conventional numerical techniques, such as finite element, finite volume and finite difference methods. In particular the VM is extremely adequate for the simulation of external flows around bluff and streamlined bodies, such as circular cylinders (Slaouti and Stansby, 1992; Koumoutsakos and Leonard, 1995; Mustto *et al*., 2000), ellipses (Akbari and Price, 2000), airfoils (Akbari and Price, 2003; Silva *et al*., 2005), bridge decks (Larsen and Walther, 1997), flapping wings of birds and insects (Eldredge, 2007) and others. Excellent reviews about the vortex method and applications can be found in Leonard (1980), Sarpkaya (1989) and Barba *et al*. (2005). We analyze the flow around a NACA 0012 airfoil that is immersed in a high Reynolds-number oscillatory freestream flow, with $Re = 1.7\times10^5$. The results show interesting features of the flow as the oscillatory numerical parameters are varied.

2. MATHEMATICAL FORMULATION

2.1. Governing equations and boundary conditions

The Vortex Method (VM) is a numerical model for the simulation of incompressible flows that solves the vorticity transport equation in terms of the vorticity field, instead of solving directly the Navier-Stokes equations in terms of the velocity field. The VM is based on the discretization of the vorticity field into a cloud of vortices (or vortex blobs) and the motion of each individual vortex is tracked within a lagrangian description, producing a method that is purely mesh-free (Chorin, 1973; Lewis, 1991; Cottet and Koumoutsakos, 2000; Kamemoto, 2004). The superposition of these blob motions allows for the determination of the velocity field from the Biot-Savart law.

Within the VM framework, the Navier-Stokes and the continuity equations are replaced by the vorticity transport equation, which can be written in nondimensional form, for two-dimensional flows, as

$$\frac{\partial \omega}{\partial t} + \mathbf{u}\cdot\nabla\omega = \frac{1}{Re}\nabla^2\omega\,, \tag{1}$$

where $\mathbf{u}$ is the velocity vector field and ω is the only non-zero component of the vorticity vector field, which is normal to the plane of the flow in two-dimensional flows. Equation (1) is nondimensionalized by the characteristic velocity, length and time scales given by U_∞, the freestream velocity, c, the airfoil chord length, and c/U_∞, respectively. The Reynolds number is defined as $Re \equiv U_\infty c/\nu$, where ν is the fluid kinematic viscosity. This equation expresses the transport of vorticity by convection and diffusion and has the property that the pressure term does not appear explicitly, allowing the velocity field to be calculated without the knowledge of the pressure field.

The flow is accelerated impulsively from rest up to the freestream flow $\mathbf{u}_\infty$ and the solution of Eq. (1) requires that the no-penetration and the no-slip boundary conditions be imposed on the airfoil solid surface, in addition to the condition that the flow tends to $\mathbf{u}_\infty$ at infinity. Mathematically, we have

$$\mathbf{u} = \mathbf{0}, \text{ on the airfoil surface;} \tag{2a}$$
$$\mathbf{u} = \mathbf{u}_\infty\,, \text{ at infinity.} \tag{2b}$$

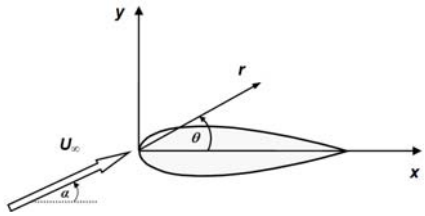

Figure 1. Flow configuration over the NACA 0012 airfoil.

2.2. The freesteam flow

We assume that the airfoil is fixed and set at a geometrical angle of attack α and that the freestream $\mathbf{u}_\infty$ possesses a lateral oscillatory component. Hence, the x- and y-components of $\mathbf{u}_\infty$ can be expressed in nondimensional form as

$$u_\infty = \cos\alpha \quad \text{and} \quad v_\infty = \sin\alpha + KC\, f_e \cos(2\pi f_e t)\,, \tag{3a,b}$$

where KC is the Keulegan-Carpenter number and f_e is the (nondimensional) excitation frequency, defined as

$$KC \equiv \frac{2\pi A_\infty}{c} \quad \text{and} \quad f_e \equiv \frac{f_e^* c}{U_\infty}\,. \tag{4a,b}$$

In Eqs. (4), A_∞ denotes the amplitude of the periodic freestream flow, f_e^* is its dimensional excitation frequency, and t is the nondimensional time. A quantity directly related to f_e that is commonly used in the analysis of oscillatory flow problems is the reduced frequency, defined as $k \equiv 2\pi f_e$. Equations (3) reduce to $u_\infty = 1.0$ and $v_\infty = KC\, f_e \cos(2\pi f_e t)$, respectively, for the particular case where the angle of attack is zero. The excitation frequency is an input parameter of the simulations and it is physically different from the vortex shedding frequency f_v, which is expressed in nondimensional form by the Strouhal number, that is, $St \equiv f_v c / U_\infty$.

3. THE DISCRETE VORTEX METHOD

3.1. The vorticity equation and the velocity field

Equation (1) can be solved by the VM using the operator splitting algorithm proposed by Chorin (1973). The idea is to decompose Eq. (1) into two equations, one purely convective and one purely diffusive, such that they are solved sequentially within the same time step. Thus, Eq. (1) is replaced in the numerical algorithm by

$$\frac{\partial\omega}{\partial t} + \mathbf{u}\cdot\nabla\omega = 0 \quad \text{and} \quad \frac{\partial\omega}{\partial t} = \frac{1}{Re}\nabla^2\omega\,. \tag{5a,b}$$

The solution of Eqs. (5) is obtained by the superposition of vortices (or vortex blobs) that move in a lagrangian manner to satisfy Eq. (5a) and that, simultaneously, suffer a diffusion process to satisfy Eq. (5b). The velocity field of each vortex must be expressed as a function of the vorticity field. In incompressible flows, the velocity field induced by the vorticity field concentrated in a finite region is determined by the Biot-Savart law (Batchelor, 1967). For the two-dimensional case of a point vortex, the velocity induced in the θ-direction, with clockwise circulation considered positive, is given by $u_\theta(r) = -\Gamma/2\pi r$, where the circulation Γ is the vortex strength and r is the radial distance from the vortex to the point of interest. If a vortex is localized at a point P(x_0,y_0), the Cartesian components of the velocity field in the x and y-directions, respectively, are

$$u = \frac{\Gamma}{2\pi}\frac{(y-y_0)}{\sqrt{(x-x_0)^2+(y-y_0)^2}} \quad \text{and} \quad v = -\frac{\Gamma}{2\pi}\frac{(x-x_0)}{\sqrt{(x-x_0)^2+(y-y_0)^2}}\,. \tag{6a,b}$$

Equations (6) present a singularity as point P(x_0,y_0) is approached. We remove this singularity at the center of the vortex using a Lamb vortex, as discussed in section 3.4.

3.2. The panel method

For the potential flow, the velocity field can be written as the gradient of a scalar velocity potential, $\mathbf{u} = \nabla\phi$. The velocity potential ϕ is a solution of Laplace´s equation, obtained from the substitution of the equation above into the continuity equation for incompressible flow. Thus, we can write

$$\nabla^2\phi = 0\,, \quad \text{in the fluid region.} \tag{7}$$

Equation (7) is subject to the no-penetration boundary condition, $\nabla\phi\cdot\mathbf{n} = 0$, on the airfoil surface, and the boundary condition at infinity, $\nabla\phi = \mathbf{u}_\infty$. This boundary value problem is solved using the panel method, originally devised by Martensen (1971), and it is described in detail by Katz and Plotkin (2001). The panel method has the advantage that it

may be easily applied to complex geometries. The airfoil geometry is divided into straight segments, called panels, each with length Δl_i. The point in the middle of the panel is the control point, where the boundary condition must be satisfied, and the endpoints are the panel nodes. Among the possible choices for the solution of Laplace's equation, we choose the vortex singularity with linear distribution of vorticity along the panel length. The linear vortex strength is calculated so that the no-penetration boundary condition is satisfied at the control points. This formulation yields a linear system of N algebraic equations, one for each control point, and $N + 1$ unknowns, the panel vorticity strength at the panel nodes. This system needs an extra equation to be solved uniquely, which is the Kutta condition, for steady potential flows, or the conservation of circulation condition, for unsteady flows such as the ones studied here. The linear vortex distribution is employed in this work based Pereira and Bodstein (2004). The airfoil is discretized so that the leading and trailing edge regions have a fine concentration of panels, as recommended by Lewis (1991) and Katz and Plotkin (2001). In these regions, the flow experiences high velocity and pressure gradients.

3.3. Vortex shedding

The vorticity generation process in the solid-fluid interface is modeled using the solution obtained for the vorticity distribution on the panels. Once the vorticity distribution is found, discrete vortex blobs are generated near the solid surface, with strength equal to the mean vorticity on the panel $[(\gamma_i + \gamma_{i+1})/2]\Delta l_i$ and positioned at a small distance ε perpendicular to each panel control point, as shown in Fig. 2. These vortices are free to be convected and diffused by the flow, simulating the vorticity shedding process into the wake. The value of ε is based on the Lamb vortex core (Mustto *et al*., 2000), and we use the value $\varepsilon = \sigma_0 = 0.005$ in our simulations.

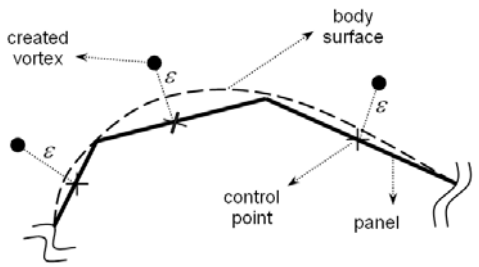

Figure 2. Vorticity shedding from the body surface.

3.4. Vorticity convection and diffusion

The calculation of the convective velocity field requires the calculation of the induced velocities of each vortex, which are modeled using Lamb vortices to avoid the singular behavior presented by point vortices, as one can see from Eqs. (6). The velocities induced by a vortex j at a point (x_i,y_i) of the fluid domain can be written as

$$u_{ij} = \begin{cases} \Gamma_j U_{ij} & \text{if} \quad r_{ij} \geq \sigma_0 \\ \Gamma_j U_{ij}\left[1-\exp\left(-5.02572(r_{ij}/\sigma_0)^2\right)\right] & \text{if} \quad r_{ij} < \sigma_0 \end{cases}, \tag{8a}$$

$$v_{ij} = \begin{cases} \Gamma_j V_{ij} & \text{if} \quad r_{ij} \geq \sigma_0 \\ \Gamma_j V_{ij}\left[1-\exp\left(-5.02572(r_{ij}/\sigma_0)^2\right)\right] & \text{if} \quad r_{ij} < \sigma_0 \end{cases}, \tag{8b}$$

where $U_{ij} = \dfrac{1}{2\pi}\dfrac{y_i - y_j}{r_{ij}^{\,2}}$, $V_{ij} = -\dfrac{1}{2\pi}\dfrac{x_i - x_j}{r_{ij}^{\,2}}$, $r_{ij} = \sqrt{\left(x_i - x_j\right)^2 + \left(y_i - y_j\right)^2}$. (9a,b,c)

In Eqs. (8a,b), Γ_j is the vortex strength and σ_0 is the vortex core radius. The total induced velocity must be calculated adding three different contributions: the first from the vortex cloud; the second from the panels, which represent the body influence on the flow; and the last one from the freestream velocity field $\mathbf{u}_\infty$.

The vorticity diffusion process is simulated using the Random Walk Method (Lewis, 1991). Equation (5b) has an analytical solution for the vorticity field of a point vortex that is initially irrotational and whose vorticity spreads out purely by the action of viscosity. This solution is given by

$$\omega(r,t) = Re\frac{\Gamma}{4\pi t}\exp\left[-Re\frac{r^2}{4t}\right], \tag{10}$$

where $r = (x^2 + y^2)^{1/2}$. Since the vorticity field is expressed as the superposition of a large number of vortices, Eq. (10) can be interpreted as the probability to find a vortex at a given spatial region at a given time (Lewis, 1991). Under this assumption, the diffusive displacements of each vortex in the x and y directions can be expressed as

$$\Delta x_D = \Delta r\cos(\Delta\theta) \text{ and } \Delta y_D = \Delta r\,\mathrm{sen}(\Delta\theta), \tag{11a,b}$$

where the radial and circumferential displacements are obtained from $\Delta r = [(4\Delta t / Re)\ln(1/P)]^{1/2}$ and $\Delta\theta = 2\pi Q$. The quantities P e Q are random numbers between 0 and 1 drawn from a uniform probability density distribution.

To calculate the convective displacement of the vortices in the x and y directions, we use we use the first-order Euler scheme for the first step of the nascent vortices, given, respectively, by $\Delta x_C = u(t)\Delta t$ and $\Delta y_C = v(t)\Delta t$, and a second-order Adams-Bashforth time-marching scheme for the reaming steps of all vortices, given by

$$\Delta x_C = \left[1.5u(t) + 0.5u(t-\Delta t)\right]\Delta t \text{ and } \Delta y_C = \left[1.5v(t) + 0.5v(t-\Delta t)\right]\Delta t\ . \tag{12a,b}$$

As soon as the diffusive and convective displacements are determined, the new vortex cloud position is evaluated according to

$$x(t+\Delta t) = x(t) + \Delta x_D + \Delta x_C \text{ and } y(t+\Delta t) = y(t) + \Delta y_D + \Delta y_C\ . \tag{13a,b}$$

In this study, vortices that penetrate into the body are reflected back into the flow, retaining a larger wake resolution and providing better quality of the results.

3.5. Aerodynamic loads

The loads on the body surface are determined from

$$\frac{\partial u_s}{\partial t} = -\frac{1}{2}\frac{\partial p}{\partial s}, \tag{14}$$

where s denotes the direction that is tangential to body surface. A circulation balance around a panel shows that the tangential velocity at a control point is given by $u_s = -\gamma$. With this result, Eq. (14) can be written in discretized form as

$$\Delta p_k = \frac{2\gamma_k \Delta l_k}{\Delta t}\ . \tag{15}$$

Equation (15) furnishes the increase in pressure at the control point of the kth panel due to the variation of circulation in time. Integrating this equation along the body surface, having p_{ref} as an arbitrary reference pressure, yields

$$p_i = p_{ref} + \sum_{k=1}^{i}\Delta p_k\ . \tag{16}$$

Without loss of generality we choose the reference pressure $p_{ref} = 0$. Equation (16) allows each p_i to be calculated at the corresponding i^{th} control point, and the maximum value of p_i on the body, p_0, becomes the stagnation pressure. Adding the quantity $(1 - p_0)$ to the values of p_i, we obtain the pressure coefficient on the airfoil surface, C_p. Integrating C_p over the body surface and projecting the loads along the parallel and perpendicular flow directions produce the drag and lift coefficients, respectively, which are given by

$$C_l = \sum_{i=1}^{N} C_{pi}\,\Delta l_i\,\mathrm{sen}(\alpha+\beta_i) \text{ and } C_d = \sum_{i=1}^{N} C_{pi}\Delta l_i\cos(\alpha+\beta_i), \tag{17a,b}$$

where Δl_i is the length and β_i is the inclination of the ith panel with respect to the x-axis.

3.6. Numerical considerations

For the solution of the linear system of algebraic equations, an extra equation must be added in order to render the system determined and the solution unique. As pointed out previously, we include an equation for the conservation of circulation that expresses Kelvin's theorem. This equation may be written as

$$\sum_{j=1}^{N} \frac{\gamma_j + \gamma_{j+1}}{2} \Delta\ell_j + \sum_{k=1}^{M} \Gamma_k = 0 \,, \tag{18}$$

where N is the number of panels and M is the number of discrete vortices in the vortex cloud, each one with vortex strength Γ_k. Since the fluid flow begins from rest, there are no vortices in the wake at the first time step. Hence, Eq. (18) reduces to

$$\sum_{j=1}^{N} \frac{\gamma_j + \gamma_{j+1}}{2} \Delta\ell_j = 0 \,. \tag{19}$$

In the following time step, the linear vortex distributions along the body panels are transformed into Lamb vortices, each with strength $\Gamma_k = [(\gamma_i + \gamma_{i+1})/2]\Delta l_i$ and whose sum over all the N vortices is equal to zero due to Eq. (19). Therefore, the second term in Eq. (18) is zero, and again it reduces to Eq. (19). Thus, Eq. (19) is the one that is used to complete the linear system of algebraic equations. The solution is found using a LU decomposition algorithm.

Another special consideration that must be made concerns the velocities induced at the control points from vortices too close to the body, and vice-versa, velocities from body panels induced at vortices that are too close to the control points. In both cases, these induced velocities may be unrealistically high, requiring special treatment. Following Lewis (1991), we adopt the following procedure based on the distance from the vortex to the nearest control point r_{jk}. For a panel of length Δl_k, if $r_{jk} < 0.4\ \Delta l_k$, that is, if the vortex is extremely close to the control panel, we use the velocity induced by its image inside the body, located the same distance apart from the panel in the normal direction, to compute the velocity induced at the vortex. If the vortex is a little farther from the control point, in the range $0.4\ \Delta l_k \le r_{jk} < 2.0\ \Delta l_k$, the panel is divided into 5 subpanels, and the induced velocities at the vortex are computed as the sum of the contributions of all subpanels, whereas the velocity at the control point is the average of the velocity induced by the vortex at the control points of each subpanel. If the vortex is even farther, that is, $r_{jk} > 2.0\ \Delta l_k$, the velocity field is calculated using the equations described in the sections above. This simple model has added important improvements to the accuracy of the complete algorithm employed in this work.

4. RESULTS AND DISCUSSION

In this section we present a sequence of numerical simulations for a NACA 0012 airfoil for a zero-degree angle of attack, $\alpha = 0$, and several values of the Keulegan-Carpenter number, KC, and the (nondimensional) excitation frequency, f_e. In all cases, the number of panels remains constant and equal to 300 and the time-step is $\Delta t = 0.05$. We display all the results at $t = 17.5$ and we zoom into the wake around the airfoil region. The Reynolds number used in the simulations is 1.7×10^5.

Figure 3 shows the results obtained from the simulations. Figure 3(a) is a reference case run without the oscillatory flow component, i. e., $KC = f_e = 0$, and, therefore, the freestream flow is uniform. We can observe that the wake possesses a relatively narrow lateral extension, a characteristic that is typical of the wake of a streamlined body, and an oscillatory behavior of high frequency. The (small) oscillation period observed in the temporal variation of the lift-coefficient curve is of order $T = 0.5$, or $St = 2$. The drag-coefficient frequency of oscillation fluctuates at twice the frequency of the lift coefficient, as expected, because the drag force reaches two peaks of maximum (or minimum) for every maximum peak of the lift force. For large time, say $t = 10$, the (small) amplitude if oscillation remains within the ±0.1 envelope for C_L and less than ±0.005 for C_D. This periodic high-frequency low-amplitude fluctuation is associated with the alternate vortex shedding from the airfoil surface. A vortex is shed from the top of the airfoil surface, creating suction and causing the body to experience non-zero lift. After half a cycle is elapsed, an alternate vortex is created at the lower surface. Averaging over a cycle, the body experiences non-zero drag and zero lift, but since the temporal variation is periodic, the non-zero amplitude of oscillation produces cyclic loads on the airfoil.

Figures 3(b) – 3(e) show, qualitatively and quantitatively, the effect of the variation of KC and f_e, taken both as input data in the computations, on the vortex shedding mechanism, and, therefore, on the airfoil forces and wake development. The nondimensional excitation period, T_e, corresponds to the inverse of the excitation frequency, $T_e = 1/f_e$. The first result that can be clearly noted in all curves of the lift coefficient is that the vortex shedding frequency, measured by the Strouhal number, St, and calculated as the inverse of the vortex shedding period, $St = 1/T_v$, is exactly

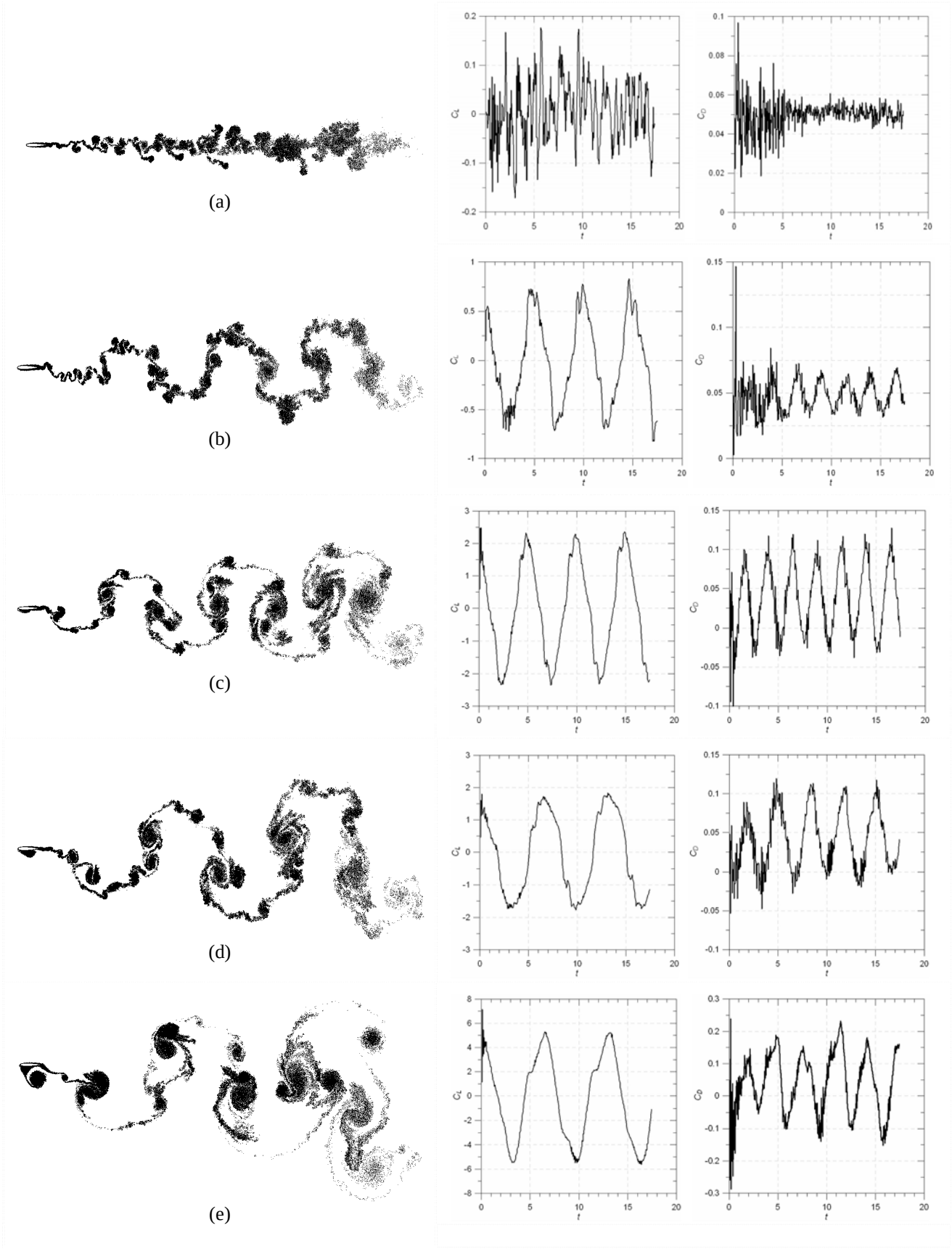

Figure 3. Position of the wake vortices at t = 17.5 for NACA 0012 airfoil and time histories of C_L and C_D, for $Re = 1.7\times10^5$ and $\alpha = 0^o$: (a) $KC = 0, f_e = 0$; (b) $KC = 1.00, f_e = 0.20$; (c) $KC = 3.00, f_e = 0.20$; (d) $KC = 3.00, f_e = 0.15$; (e) $KC = 7.50, f_e = 0.15$.

equal to the excitation frequency. This fact can be deduced directly from the oscillation period T_v observed in the graph for the temporal variation of the lift coefficient. For the cases where f_e = 0.20, which corresponds to T_e = 5.0, the oscillation period obtained from the curve of C_L against t is also T_v = 5.0, and for the case with T_e = 6.67, the vortex shedding obtained is also T_v = 6.67. This observation indicates that if the body is flexible and oscillates with frequency $f_e = St$ and these two frequencies match the body natural frequency, there occurs the phenomenon known as "lock-in", which may cause severe damage to the body.

On the other hand, the Keulegan-Carpenter number, which nondimensionalizes the oscillatory flow amplitude, have a direct influence on the wake and the oscillation amplitudes of the force coefficients. The figures that illustrate the wake pattern in the final instant of simulation have shown a larger lateral extension when compared with the reference case (without oscillation), and this lateral extension increases when *KC* increases, keeping the excitation frequency constant. This phenomenon is observed in all cases simulated. The fact that the oscillation amplitude of the force coefficients increases when *KC* increases is very significant. Specifically, in comparison with the reference case, the results of Figs. (3b) and (3c), where *KC* takes the values *KC* = 1 and 3 and f_e = 0.20, respectively, the oscillation amplitudes of C_L and C_D, are approximately 0.75 and 0.02, respectively, for the case of Fig. 3(b), and 2.25 and 0.06 for the case of Fig. 3(c). These results indicate that, in the range of values studied, an increase of *KC* induces a linear increase on both forces coefficients. Similar results are observed for the simulation with f_e = 0.15, illustrated in Figs. 3(d) and 3(e). If we keep the value of *KC* constant and equal to 3 and decrease the value of f_e, the wake have a smaller number of oscillations and the Strouhal number diminish. In both cases, *St* is again equal to f_e. This behavior can be observed when we compare Figs. 3(c) and 3(d). We also notice that the relation between the oscillation frequencies of the two curves present, for all oscillatory flow cases, the same behavior as the non-oscillatory case. More specifically, the results for the oscillatory flow cases show that the drag coefficient curve oscillates with a frequency twice as large as the oscillation frequency of the lift coefficient. In other words, the oscillatory component of the freestream flow does not modify, in the range of parameters studied, the relation between the oscillation frequencies of both force coefficients.

The set of simulations discussed in this paper allows us to infer that, maybe with the exception for the case of lowest non-zero value of *KC* – Fig. 3(b), all the other cases seem to indicate the occurrence of dynamic stall. This phenomenon is characterized by the occurrence of separation on the leading edge of the airfoil, forming a leading-edge vortex that increases the suction on the surface of the airfoil and causes an increase of the normal force beyond the static stall angle of attack. Due to the periodic variation of the incoming flow, the transverse oscillatory velocity component induces a momentary increase of the effective angle of attack to a value beyond the static stall angle, causing separation and the formation of the leading-edge vortex. Ultimately, stall occurs. As soon as the transverse velocity component inverts its sign, the stall disappears and another leading-edge vortex starts to develop on the other side of the airfoil. This process repeats itself over the oscillation cycle and may cause massive mechanical loads to appear on the airfoil surface. As we can see in Figs. 3(c)-(e), a leading-edge vortex is clearly displayed on the lower side of the airfoil, which increases as *KC* increases. Figure 3(e) show the largest leading-edge vortex, since it corresponds to the highest *KC* value, which means that the local angle of attack is the largest for all cases studied. This behavior is qualitatively similar to the dynamic stall phenomenon that happens in the flow around a pitching airfoil, as discussed in Akbari and Price (2003).

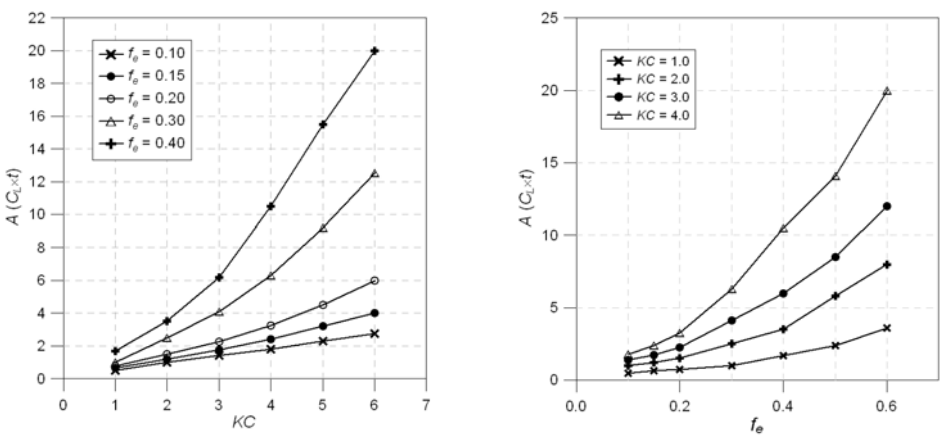

(a) (b)

Figure 4. Variation of the oscillation amplitude *A* with: (a) *KC*, for f_e constant; (b) f_e, for *KC* constant.

Figures 4(a) and 4(b) show the behavior of the oscillation amplitude, *A*, obtained from the lift-coefficient curves, plotted against *KC* and f_e, respectively. In Fig. 4(a), where the excitation frequency is held constant, we notice that the oscillation amplitude increases linearly with *KC* for the lowest values of f_e. As f_e increases, the amplitude shows a non-

linear behavior and increases more quickly. As the *KC* values are held constant and f_e increases, we observe the same pattern as in the previous case, where *A* is approximately linear when *KC* = 1.0, but increases non-linearly with f_e for higher values of *KC*. The results presented in Fig. (4) indicate that high *KC* and f_e values have a non-linear effect on the loading amplitude response.

5. CONCLUSIONS

This paper describes vortex-method simulations of an oscillating freestream flow around a NACA 0012 airfoil for $Re = 1.7\times10^5$ and $\alpha = 0$. The results indicate that, in the range of values chosen for the Keulegan-Carpenter number, *KC*, and the excitation frequency, f_e, the oscillatory component of the freestream flow does not modify the observation for non-oscillating flows that the drag coefficient oscillates with twice the frequency of the lift coefficient. It was also shown that *KC* and f_e have a direct influence over the wake development and the oscillation amplitudes of the force coefficients. As we can infer from the temporal variation of the lift and drag coefficients, the amplitude of oscillation increases as the value of *KC* and f_e increase. This behavior is linear for the lower values of *KC* and f_e and non-linear for the higher values. We also observe that the vortex shedding frequency is equal to the excitation frequency in all cases studied. For the higher values of *KC* used in the simulations, the boundary layer undergoes a large temporal variation, going from attached to massively separated conditions when the local angle of attack reaches high values. This behavior is similar to dynamic stall.

The results obtained with our simulations show that the numerical modeling employed is capable of providing simulations that represent accurately the oscillatory phenomena that occurs in this class of flows. Specifically, wind turbines in regular operation are subject to the conditions here investigated, either because of turbulent freestream flows or because of shadow effects, and this kind of fluid dynamic tool can be used in the analysis of the wind turbine performance.

6. ACKNOWLEDGEMENTS

The authors would like to acknowledge the financial support from CAPES and CNPq.

7. REFERENCES

Akbari, M.H. and Price, S.J., 2000, “Simulation of the Flow Over Elliptic Airfoils Oscillating at Large Angles of Attack”, Journal of Fluids and Structures, Vol.14, pp. 757-777.

Akbari, M.H., Price, S.J., 2003, “Simulation of Dynamic Stall for a NACA 0012 Airfoil Using a Vortex Method”, Journal of Fluids and Structures, Vol.17, pp. 855-874.

Barba, L.A., Leonard, A. and Allen, C.B., 2005, “Advances in Viscous Vortex Methods – Meshless Spatial Adaptation Based on Radial Basis Function Interpolation”, International Journal for Numerical Methods in Fluids, Vol.47, pp. 387-421.

Batchelor, G.K., 1967, “An Introduction to Fluid Dynamics”, Cambridge University Press, Cambridge, 615 p.

Chorin, A.J., 1973, “Numerical Study of Slightly Viscous Flow”, Journal of Fluid Mechanics, Vol.57, pp. 785-796.

Cottet, G.-H. and Koumoutsakos, P., 2000, “Vortex Methods: Theory and Practice”, Cambridge University Press, Cambridge, 328 p.

Eldredge, J.D., 2007, "Numerical Simulation of the Fluid Dynamics of 2D Rigid Body Motion with the Vortex Particle Method", Journal of Computational Physics, Vol.221, pp. 626-648.

Kamemoto, K., 2004, “On Contribution of Advanced Vortex Element Methods toward Virtual Reality of Unsteady Vortical Flows in the New Generation of CFD”, Journal of the Brazilian Society of Mechanical Sciences and Engineering, Vol.26, No. 4, pp. 368-378.

Katz, J. and Plotkin, A., 2001, “Low-Speed Aerodynamics”, 2nd Edition, Cambridge University Press, Cambridge, 613 p.

Koumoutsakos P. and Leonard A., 1995, “High-Resolution Simulations of the Flow around an Impulsively Started Cylinder Using Vortex Methods”, Journal of Fluid Mechanics, Vol.296, pp. 1-38.

Larsen, A. and Walther, J.H., 1997, “Aeroelastic Analysis of Bridge Girder Sections Based on Discrete Vortex Simulations”, Journal of Wind Engineering and Industrial Aerodynamics, Vol.67&68, pp. 253-265.

Leonard, A., 1980, “Vortex Method for Flow Simulation”, Journal of Computational Physics, Vol.37, pp. 289-335.

Lewis, R.I., 1991, “Vortex Element Methods for Fluid Dynamic Analysis of Engineering Systems”, Cambridge University Press, Cambridge, 592 p.

Martensen, E., 1971, “The Calculation of the Pressure Distribution on a Cascade of Thick Airfoils by Means of Fredholm Integral Equation of the Second Kind”, NASA TT F-702.

Mustto A.A., Bodstein G.C.R. and Hirata M.H., 2000, “Vortex Method Simulation of the Flow around a Circular Cylinder”, AIAA Journal, Vol.38, No. 6, pp. 1100-1102.

Pereira, L.H.G. and Bodstein, G.C.R., 2004, "Método dos Painéis com Distribuições de Singularidade Quadráticas Aplicados a Escoamentos Bidimensionais sobre Aerofólios", ENCIT – X Congresso Brasileiro de Ciências Térmicas, Rio de Janeiro, RJ, Brasil.

Sarkar, S. and Venkatraman, K., 2008, "Influence of Pitching Angle of Incidence on the Dynamic Stall Behavior of a Symmetric Airfoil", European Journal of Mechanics B/Fluids, Vol.27, pp. 219-238.

Sarpkaya, T., 1989, "Computational Methods with Vortices - The 1988 Freeman Scholar Lecture", Journal of Fluids Engineering, Vol.111, pp. 5–52.

Slaouti, A. and Stansby, P.K., 1992, "Flow around two Circular Cylinders by the Random-Vortex Method", Journal of Fluids and Structures, Vol.6, pp. 641-670.

Silva, D.F.C., Pereira, L.H.G. and Bodstein, G.C.R., 2005, "Numerical Calculation of the Unsteady Two-Dimensional Incompressible Flow around NACA Airfoils Using the Vortex Method", Proceedings of the 18th International Congress of Mechanical Engineering, Vol.1, Ouro Preto, Brazil, pp. 1-8.

Williamson, C.H.K. and Govardhan, R., 2004, "Vortex-Induced Vibrations", Annual Review of Fluid Mechanics, Vol.36, pp. 413–55.

8. RESPONSIBILITY NOTICE

The authors are the only responsible for the printed material included in this paper.